SYNTHETIC BIOLOGY

Decoding CAR T cell phenotype using combinatorial signaling motif libraries and machine learning

Kyle G. Daniels[1,2], Shangying Wang[3,4], Milos S. Simic[1,2], Hersh K. Bhargava[1,2], Sara Capponi[3,4], Yurie Tonai[1,2], Wei Yu[1,2], Simone Bianco[3,4]†*, Wendell A. Lim[1,2,4]*

Chimeric antigen receptor (CAR) costimulatory domains derived from native immune receptors steer the phenotypic output of therapeutic T cells. We constructed a library of CARs containing ~2300 synthetic costimulatory domains, built from combinations of 13 signaling motifs. These CARs promoted diverse human T cell fates, which were sensitive to motif combinations and configurations. Neural networks trained to decode the combinatorial grammar of CAR signaling motifs allowed extraction of key design rules. For example, non-native combinations of motifs that bind tumor necrosis factor receptor–associated factors (TRAFs) and phospholipase C gamma 1 (PLCγ1) enhanced cytotoxicity and stemness associated with effective tumor killing. Thus, libraries built from minimal building blocks of signaling, combined with machine learning, can efficiently guide engineering of receptors with desired phenotypes.

Chimeric antigen receptors (CARs) have demonstrated the power of synthetic signaling receptors as tools to reprogram immune cells to execute therapeutic functions, such as targeted killing of tumor cells (*1*). The antitumor efficacy of CARs is strongly modulated by the signaling domains that they contain. Current clinically approved CARs contain a core T cell receptor (TCR) signaling domain from CD3ζ [containing immunoreceptor tyrosine-based activation motifs (ITAMs) that recruit the kinase ZAP70] (*2*–*4*), along with a costimulatory signaling domain from either the CD28 (*5*, *6*) or 4-1BB (*7*) costimulatory immune receptors (*8*–*10*). The costimulatory domains are themselves composed of multiple signaling motifs, which are short peptides that bind to specific downstream signaling proteins, often through modular protein interaction domains [e.g., Src homology 2 (SH2), Src homology 3 (SH3), or other domains (*11*, *12*)]. Such peptide signaling motifs (referred to as linear motifs) are the fundamental building blocks that control the output of most signaling receptors. The constellation of signaling proteins recruited by a particular array of signaling motifs upon receptor stimulation is thought to shape the distinct cellular response. For example, in CARs, the 4-1BB costimulatory domain, which contains binding motifs for tumor necrosis factor receptor–associated factor (TRAF) signaling adaptor proteins, leads to increased T cell memory and persistence; the CD28 costimulatory domain, which contains binding motifs for phosphatidylinositol-3-kinase (PI3K), growth factor receptor-bound protein 2 (Grb2), and lymphocyte-specific protein tyrosine kinase (Lck), is associated with more effective T cell killing but reduced long-term T cell persistence (*13*). Thus, signaling motifs can be thought of as the "words" that are used to compose the phenotypic "sentences" communicated through signaling domains.

A major and still mostly outstanding goal in synthetic biology is to predictably generate new cell phenotypes by altering receptor composition. For example, in cancer immunotherapy, a general goal is not only to enhance T cell antitumor cytotoxicity but also to maintain a stem-like state associated with longer-term T cell persistence. Such a phenotype is associated with effective and durable tumor clearance (higher stemness is correlated with more resistance to T cell exhaustion). Libraries of costimulatory domains have been screened for improved phenotypes (*14*–*16*). However, the costimulatory domains used were from natural immune receptors (i.e., alternative preexisting sentences, to use the analogy to language). We propose that a more effective way to scan phenotypic space for synthetic receptors is to create libraries that sample new combinations of signaling motifs. Such an approach could, in principle, yield phenotypes that extend beyond those that can be generated by native receptor domains alone. Moreover, exploration of a broader range of receptor "motif space" could lead to a more systematic understanding of how different parameters of output are encoded by motif identity, combination, and order.

We recombined 13 signaling motifs (words) to create a CAR costimulatory domain library with randomized motif combinations (new sentences) (Fig. 1). This library of new signaling sentences produced a range of phenotypes, including combinations of phenotypes that are not observed with native signaling domains. We used neural networks to decode the language of signaling motifs, create predictive models, and extract design rules that inform the engineering of CAR signaling domains that increase cytotoxicity and stemness.

Results

A CAR library with synthetic combinations of signaling motifs generates diverse CAR T cell cytotoxicity and memory potential

To construct a combinatorial library of CAR signaling domains, we searched the Eukaryotic Linear Motif (ELM) database (*17*) and primary literature to curate a collection of 12 peptide motifs from natural signaling proteins that recruit key downstream signaling proteins that function in T cell activation. The motifs in the library recruit proteins such as phospholipase C gamma 1 (PLCγ1), TRAFs, Grb2, Grb2-related adaptor downstream of Shc (GADS), Src homology region 2 domain–containing phosphatase (SHP-1), vav guanine nucleotide exchange factor 1 (Vav1), PI3K, Lck, and Pellino protein. For example, library motif 1 is derived from the linker for activation of T cells (LAT) and contains the core motif YLVV, which when tyrosine-phosphorylated, binds the N-terminal SH2 domain of PLCγ1 with high specificity (*18*) (Y, Tyr; L, Leu; V, Val). Motif 6 contains the motif ITYAAV from the leukocyte associated immunoglobulin-like receptor 1 (LAIR1), which binds the phosphatase SHP-1 through its SH2 domain (*19*) (I, Ile; T, Thr; A, Ala). In addition to the 12 signaling motifs, we included a spacer motif as the 13th component in the library. The combinatorial library was constructed within the context of an anti-CD19 CAR (containing an anti-CD19 extracellular single-chain variable fragment and a CD3ζ signaling domain). The synthetic costimulatory domains had either one, two, or three signaling motifs. The 13 motifs were randomly inserted in positions i, j, and k (Fig. 1) to yield 2379 different motif combinations (Fig. 1, B to E). To confirm that the library displayed sufficient phenotypic diversity, we first performed low-resolution pooled screens, in which we transduced a mixed population of $CD4^+$ and $CD8^+$ primary human T cells at low multiplicity of infection and activated the pool with Nalm 6 leukemia cells ($CD19^+$) for 8 to 9 days. We used fluorescence-activated cell sorting (FACS)–based sequencing enrichment assays to observe a diverse range of phenotypic outputs for T cell proliferation, formation of central memory T cells expressing receptor-type tyrosine-protein phosphatase C (CD45RA) and lacking L-selectin (CD62L), and T cell degranulation [lysosome-associated membrane glycoprotein 1 ($CD107A^+$) T cells, a proxy for cytotoxic response] (fig. S1). All T cells were activated with beads displaying CD3 and CD28 to allow for viral transduction,

[1]Cell Design Institute, University of California, San Francisco, San Francisco, CA 94158, USA. [2]Department of Cellular and Molecular Pharmacology, University of California, San Francisco, San Francisco, CA 94158, USA. [3]Department of Functional Genomics and Cellular Engineering, IBM Almaden Research Center, San Jose, CA 95120, USA. [4]Center for Cellular Construction, San Francisco, CA 94158, USA.
*Corresponding author. Email: sbianco@altoslabs.com (S.B.); wendell.lim@ucsf.edu (W.A.L.)
†Present address: Altos Labs, Redwood City, CA 94065, USA.

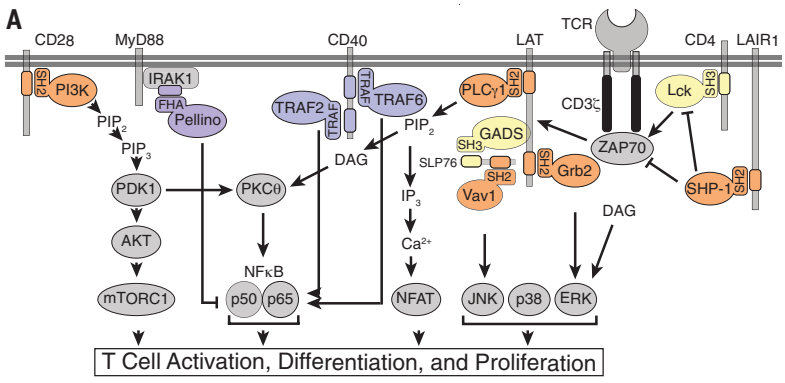

B

Library part	Source protein	Signaling motif	Binding partner	Binding domain
M1	LAT	...*YLVV*...	PLCγ1	*SH2*
M2	Gab1	...*YVPM*...	PI3K	*SH2*
M3	LAT	...*YENL*...	Grb2	*SH2*
M4	IL7Rα	...*YVTM*...*YQNQ*...	PI3K, Grb2	*SH2*
M5	SYK	...*YESP*...	Vav1	*SH2*
M6	LAIR1	...*ITYAAV*...	SHP-1	*SH2*
M7	CD4	...*PVQP*...	Lck	*SH3*
M8	SLP76	...*RSTKP*...	GADS	*SH3*
M9	CD40	...*PVQE*...	TRAF2, 3, 1	*TRAF-C*
M10	LMP1	...*PQQAT*...	TRAF2, 3, 1	*TRAF-C*
M11	CD40	...*PQEINF*...	TRAF6	*TRAF-C*
M12	IRAK1	...*RPTAVEG*...	Pellino	*FHA*
M13	synthetic	$(SAG)_6$	(spacer)	

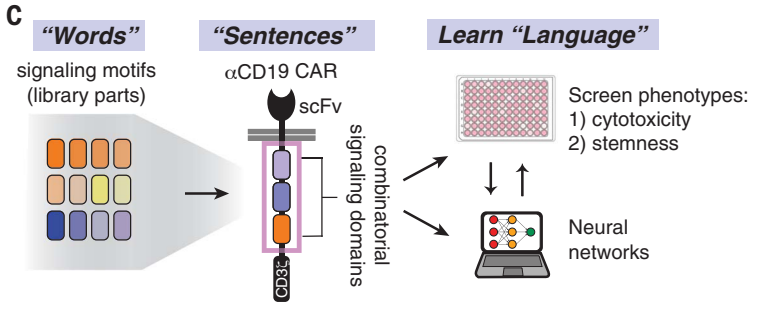

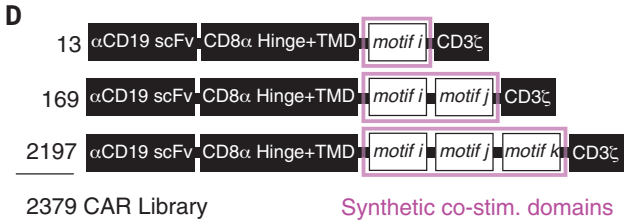

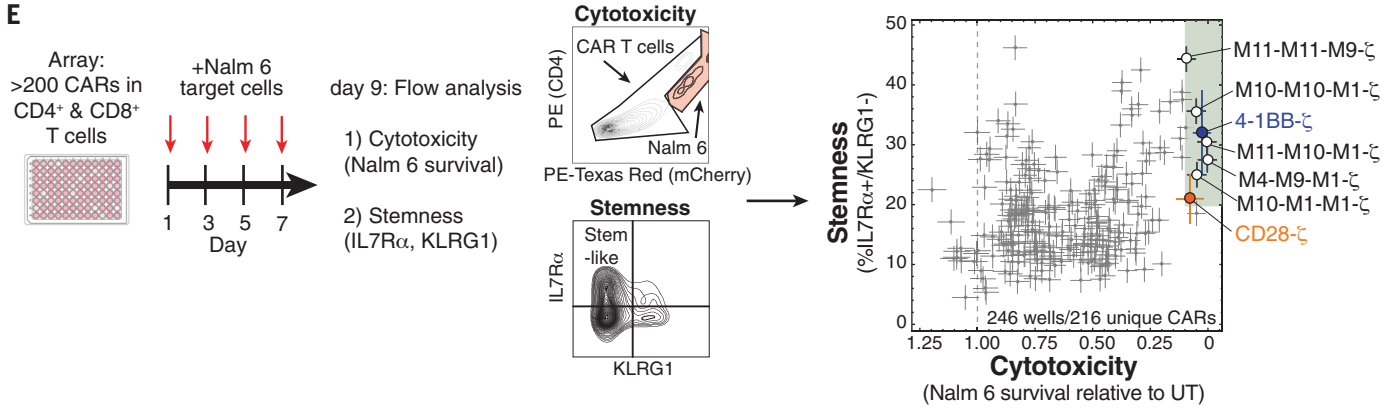

Fig. 1. CAR costimulatory domains with synthetic signaling motif combinations generate diverse cell fates with decoupled cytotoxicity and stemness. (**A**) A diverse set of proteins that function in T cell signaling are recruited by signaling motifs in the library parts. FHA, forkhead-associated domain; IP_3, inositol trisphosphate; JNK, c-Jun N-terminal kinase; mTORC1, mammalian target of rapamycin complex 1; NFAT, nuclear factor of activated T-cells; PIP_3, phosphatidylinositol 3,4,5-trisphosphate. (**B**) Description of library parts used in the combinatorial library. Each part is 16 to 18 amino acids long, including the signaling motif(s) and flanking sequence. Phospho-tyrosines are shown in bold. (**C**) New combinations of signaling motifs create distinct CAR signaling programs that control T cell phenotype. (**D**) Schematics of αCD19 CAR with variable signaling domains. (**E**) CAR T cells with various signaling motif combinations produce a broad range of cytotoxicity and stemness. $CD4^+$ and $CD8^+$ CAR T cells were pulsed four times with Nalm 6 leukemia cells and assayed for CAR T cell cytotoxicity and stemness. Errors for Nalm 6 survival and the stem-like $IL7R\alpha^+/KLRG1^-$ population in (E) were estimated by calculating the average standard deviation for seven CAR constructs with internal replicates in the array. PE, phycoerythrin; UT, untransduced.

and subsequent activation through CARs with distinctive signaling domains led to divergent phenotypes.

To screen the library at higher resolution, we transformed bacteria with library plasmid stocks and randomly picked colonies to select a subset of more than 200 CARs from the combinatorial library to characterize in an arrayed screen (Fig. 1E). An arrayed screen, in which each CAR is studied independently, was important because immune paracrine signaling could confound analysis of pooled CAR T cell screens. We activated the $CD4^+$ and $CD8^+$ CAR T cells in the arrayed screen by culturing with Nalm 6 ($CD19^+$) cells for 8 to 9 days. Four pulses of Nalm 6 cells were used to mimic longer term stimulation that can exacerbate T cell exhaustion. At the end of the coculture, we used flow cytometry to assess the cytotoxicity of the mixed $CD4^+$ and $CD8^+$ CAR T cell populations (based on Nalm 6 cell survival), stemness [interleukin-7 receptor subunit alpha ($IL7R\alpha^+$) and killer cell lectin receptor G1 ($KLRG1^-$)] (*20*–*23*), and maintenance of T cell populations with markers of central memory or naïve state (CD45RA and CD62L).

The CARs in the arrayed screen displayed a range of cytotoxicity and stemness. The total naïve and central memory population was positively correlated with cytotoxicity (fig. S2B). Stemness and the naïve population were roughly proportional across the library (fig. S2, C and D). However, cytotoxicity and stemness were uncoupled. This observation underscores the ability of unusual combinations of motifs in costimulatory domains to drive CAR T cells

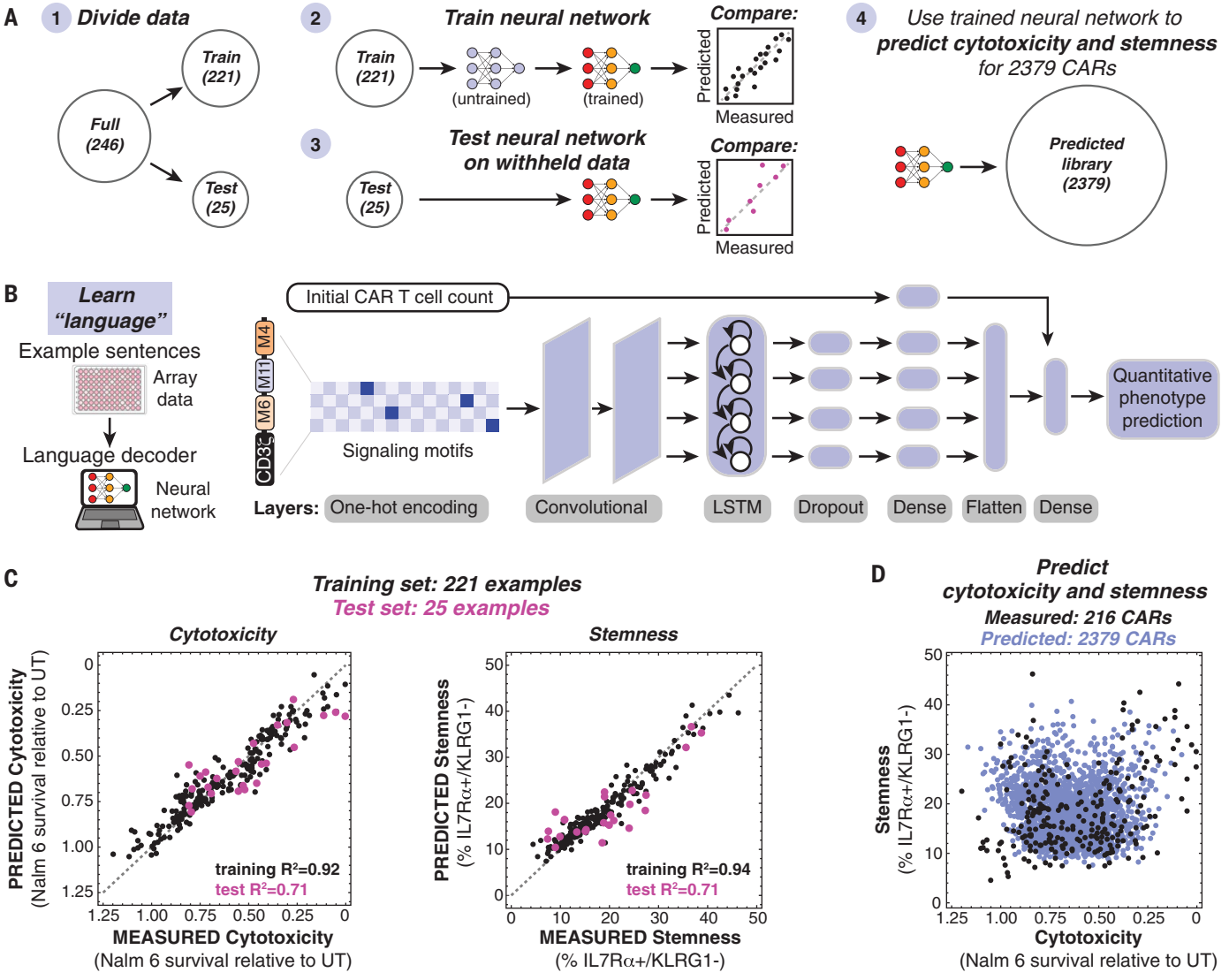

Fig. 2. Neural networks decode the combinatorial language of signaling motifs to predict cytotoxicity and stemness of motif combinations. (**A**) Array data were subdivided in datasets to train and test neural networks that were subsequently used to predict the cytotoxicity and stemness of 2379 CARs. (**B**) Schematic of the neural network used to predict CAR T cell phenotype. LSTM, long short-term memory. (**C**) Neural networks trained on array data predict the cytotoxicity and stemness of CARs in the training sets (black) and the withheld test sets (pink). The root mean squared error (RMSE) for the cytotoxicity training set is 0.07579, and the RMSE for the cytotoxicity test set is 0.1327. The RMSE for the stemness training set is 2.2038, and the RMSE for the stemness test set is 4.7941. (**D**) Trained neural networks were used to predict the cytotoxicity and stemness of 2379 CARs containing one to three variable signaling motifs. Predictions represent the mean for n = 10 neural networks with different hyperparameters.

to varied cell fates with particular combinations of phenotypes. Several costimulatory domains produced cytotoxicity and stemness comparable to that of 4-1BB. Many of these contained motifs that recruit both TRAFs (motif 9, motif 10, motif 11) and PLCγ1 (motif 1). For example, M10-M10-M1-ζ, M10-M1-M1-ζ, M11-M10-M1-ζ, and M4-M9-M1-ζ all promoted cytotoxicity and stemness.

Neural networks predict the CAR T cell cytotoxicity and memory potential encoded by combinations of signaling motifs

The diverse cytotoxicity and stemness profiles observed in our arrayed screen are consistent with a complex relationship between signaling motif combinations and arrangement and resulting T cell phenotypes. We sought to leverage the combinatorial nature of the costimulatory domain library by using machine learning to decode the "language" of signaling motifs that relates motif combinations to cytotoxicity and stemness outputs. We separated the arrayed screen data into a training set (221 examples) and a test set (25 examples). We then used these datasets to train several machine-learning algorithms to predict cytotoxicity and stemness based on costimulatory domain identity and arrangement (Fig. 2A and fig. S3). Neural networks (Fig. 2B) were best able to recapitulate the measured phenotypes in the training data (Fig. 2C) and to effectively predict the phenotypes in the test set (Fig. 2D). For both cytotoxicity and stemness training and test sets, the neural network was able to capture much of the relationship between signaling motif composition and phenotype, with coefficient of determination (R^2) values of ~0.7 to 0.9.

The trained neural networks then allowed us to predict the CAR T cell cytotoxicity and stemness that would result from each of the 2379 motif combinations in the full combinatorial library (Fig. 2D), including those that were not part of the smaller arrayed screen. These simulated 2379 CARs sample the entire combinatorial space of the library, providing a dataset from which we extracted design

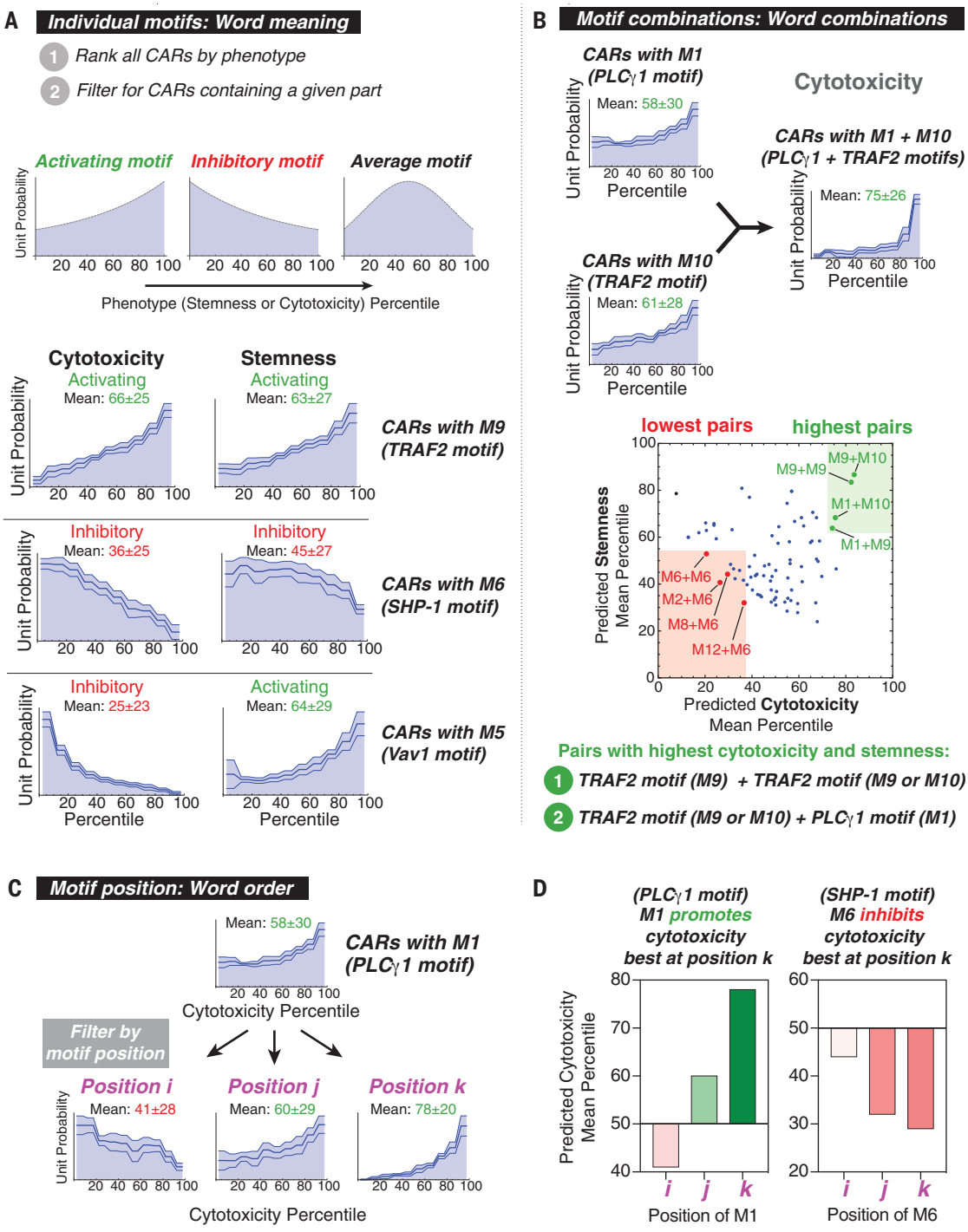

Fig. 3. Distribution analysis quantifies elements of linear motif language to extract design parameters for signaling domains. (**A**) The distribution of library parts throughout CARs in the ranked library reflects effects of signaling motifs on phenotype. Activating motifs are found in CARs with higher rank, and inhibitory motifs are found in CARs with a lower rank. The three lines within the distributions represent mean predictions ± SEM calculated from n = 10 neural networks. (**B**) CARs containing pairs of motifs that recruit TRAFs (M9 and M10) or PLCγ1 (M1) promote high cytotoxicity and stemness. Pairs promoting the highest and lowest cytotoxicity and stemness were determined by taking the sum of the mean percentile for each phenotype. (**C**) Cytotoxicity percentile distributions for CARs containing M1 at various positions demonstrate that effects of signaling motifs on phenotype are position dependent. (**D**) Position-dependence of signaling motifs is quantified by calculating the mean of percentile distributions. M1 is predicted to promote cytotoxicity best at position k, whereas M6 is predicted to inhibit cytotoxicity best at position k.

rules. We analyzed (i) the overall contribution of each motif to a particular phenotype (without regard to combinatorial context), (ii) identification of pairwise motif combinations that promote particular phenotypes, and (iii) positional dependence of motifs.

Distribution analysis summarizes the effects of signaling motifs, motif combinations, and motif positions on CAR T cell phenotype

To assess the overall contribution of individual motifs, we ranked all the CARs in our library by neural network–predicted cytotoxicity and stemness and then assessed whether motifs were enriched in the strong or weak ends of the phenotypic distribution (Fig. 3A and fig. S4). If a motif is generally activating for a phenotype, then it is expected to be more common in highly ranked CARs; if a motif is inhibitory, then it is expected to be more common in poorly ranked CARs. Although the effects observed in this distribution analysis depend on other motifs in the CAR and the position of the motif in question, the distributions are informative of the overall effect that each motif has in the context of the library. An analogous distribution analysis was also done on the pooled screening proliferation data (fig. S5).

This distribution analysis highlighted several effective motifs that have activating and inhibitory roles. For example, motif M9 is the PQVE motif [from cluster of differentiation 40 (CD40)], which binds TRAF2, and is associated with T cell activation and function (*24*, *25*) (P, Pro; Q, Gln; E, Glu). Accordingly,

M9 is enriched in CARs with high cytotoxicity (mean 66th percentile) and high stemness (mean: 63rd percentile), indicating that overall, it promotes both of these phenotypes. In a contrasting example, M6 (from LAIR1) recruits the phosphatase SHP-1, an inhibitor of T cell activation. Accordingly, M6 is enriched in CARs with low cytotoxicity (mean: 36th percentile) and low stemness (mean: 45th percentile), indicative of inhibition of both phenotypes. Some motifs can activate one phenotype and inhibit another: M5, which binds Vav1, is unrepresented in CARs with high cytotoxicity (mean: 25th percentile) but overrepresented in CARs with high stemness (mean: 64th percentile). Thus, Vav1 signaling appears to promote stemness while inhibiting killing. The quantified effects of all individual motifs on cytotoxicity and stemness are shown in the heatmap in fig. S4. The TRAF binding motifs (M9 and M10) are among the best at promoting both cytotoxicity and stemness.

We anticipated that phenotypes would be highly dependent on motif combinations, because different downstream signaling pathways could be either complementary, redundant, or competing. To examine motif pairs that favored particular phenotypes, we examined the occurrence of each possible pair (without regard to order) in the ranked distribution. Several specific motif pairs appear to promote both cytotoxicity and stemness when they occur in combination within a costimulatory domain. For example, M1 (PLCγ1) and M10 (TRAF) were each activating with respect to cytotoxicity (means: 58th and 60th percentiles), but the M1+M10 motif pair was even more strongly activating (mean: 75th percentile). The predicted mean cytotoxicity and stemness percentiles for all 144 pairs of motifs M1 to M12 are shown in Fig. 3B. The motif pairs M1+M10, M1+M9, M9+M9, and M9 +M10 were best at promoting cytotoxicity and stemness. These pairs all demonstrate that TRAF-binding motifs (M9 and M10) work well in tandem, as well as in combination with the motif that recruits PLCγ1 (M1), whose signaling activates nuclear factor kappa B (NFκB). Thus, these pathways may serve complementary roles in these phenotypes. A number of motif pairs strongly inhibited cytotoxicity and stemness. All four motif pairs with the lowest cytotoxicity and stemness contain M6, which binds the inhibitory phosphatase SHP-1.

The phenotype of CAR T cells was highly dependent on the position of a motif within the costimulatory domain (fig. S4B). For example, M1 (PLCγ1) showed strong cytotoxicity when in positions k or j and weak cytotoxicity in position i (Fig. 3, C and D). M9 (TRAF) and M10 (TRAF) showed optimal cytotoxicity and stemness when in positions i and j. This is consistent with the experimental observation that TRAF-binding parts M9 and M10 followed by M1 (in N- to C-terminal order) promote the most cytotoxicity and stemness (M1 followed by M9 or M10 does not (fig. S2E). These results indicate that shuffling motif position is an approach for calibrating phenotype.

The above distribution analysis quantifies elements of motif language, capturing the effects of motifs (word meaning), motif pairs (word combinations), and motif position (word order) on phenotype. The analysis also yields design rules that can inform combinations and arrangements of motifs that are capable of producing a desired cell fate. For example, a synthetic costimulatory domain that contains one or more TRAF binding motifs (M9 or M10) followed by a PLCγ1 (M1) motif appears to be effective at promoting both cytotoxicity and stemness (Fig. 4A). Although tandem TRAF binding motifs occur in the naturally evolved 4-1BB receptor (*26*) (fig. S6A), the combination of TRAF and PLCγ1 motifs is not found in natural characterized immune receptors. Thus, we tested whether adding PLCγ1 (M1) motifs to 4-1BB–like domains could improve phenotypes induced by CARs. Moreover, we also wanted to determine whether adding M1 might be a general strategy to improve the efficacy of other costimulatory domains, such as CD28.

Neural networks predict that the addition of M1 enhances the cytotoxicity and memory potential of 4-1BB–ζ but not CD28–ζ

We examined the neural network–predicted library to predict the effects of adding the M1 motif to CD28-like and 4-1BB–like synthetic costimulatory domains (library members whose signaling motifs shared the overall configuration of natural signaling motifs in CD28 and 4-1BB) (Fig. 4A). The 4-1BB–like costimulatory domains were predicted by the neural network model to show increased cytotoxicity and stemness, consistent with experimental observations. By contrast, addition of M1 motifs to CD28-like costimulatory domains was not predicted to enhance cytotoxicity or stemness.

To experimentally test this, we synthesized derivatives of the 4-1BB and CD28 costimulatory domains with one or two copies of the M1 motif added to the C terminus and tested the effects of these costimulatory domains on killing of Nalm 6 and maintenance of T cell stemness (Fig. 4B). Consistent with predictions, 4-1BB showed notably enhanced cytotoxicity and stemness upon addition of M1, whereas CD28 showed almost no change. Importantly, in addition to predicted in vitro changes, the 4-1BB–M1–M1–ζ CAR construct showed improved efficacy in a Nalm 6 tumor Nod scid gamma (NSG) mouse model (Fig. 4C and fig. S6). Relative to standard 4-1BB CAR T cells, the 4-1BB–M1–M1–ζ CAR T cells delayed the growth of Nalm 6 tumor cells for an additional 2 weeks, in agreement with the predictions from the library and neural network model.

Why might a PLCγ1 motif improve T cell phenotype in combination with the 4-1BB domain (TRAF motifs) but not in the context of the CD28 domain (PI3K, Grb2, Lck motifs)? PLCγ1 catalyzes the production of diacylglycerol (DAG) from phosphatidylinositol 4,5-bisphosphate (PIP_2), which activates Ras guanyl-releasing protein (RasGRP) and protein kinase C theta (PKCθ), subsequently activating the extracellular signal–regulated kinases (ERK1 and ERK2) and NFκB. This signaling is similar and possibly redundant to that of PI3K and Grb2, which also activate RasGRP and PKCθ. TRAF signaling, however, does not activate RasGRP or PKCθ, such that PLCγ1 and TRAF signaling are more likely to be complementary (Fig. 4D). We experimentally characterized the 4-1BB–M1–M1–ζ CAR construct (compared with standard 4-1BB–ζ CAR) by measuring the kinetics of phosphorylation of protein kinase B (Akt), ERK1 and ERK2, and NFκB after stimulation by Nalm 6 (Fig. 4E and fig. S7A). The addition of the M1 motifs increased phosphorylation of ERK1 and ERK2 (1.7-fold) and NFκB (2.4-fold), both of which depend on activation of PLCγ1. Phosphorylation of Akt, which is not dependent on PLCγ1, showed only a 1.2-fold increase. The observed increase in activation of NFκB and ERK1 and ERK2 supports the hypothesis that PLCγ1 signaling is complementary to TRAF signaling and is consistent with the importance of NFκB activation for the maintenance of $CD8^+$ T cell memory (*27*). By contrast, no significant increase in activation of NFκB and ERK1 and ERK2 was observed for a CAR in which the PLCγ1 motif was appended to the CD28 costimulatory domain. We observed little additional activation-induced increase in PLCγ1 phosphorylation in the cells bearing the 4-1BB–M1–M1–ζ CAR (fig. S7C), suggesting that M1 may enhance signaling by altering the precise spatial organization of PLCγ1 binding sites (*28*) or by promoting PLCγ1-dependent LAT clustering (*29*).

Conclusions

We find that signaling motif libraries and machine learning can be combined to elucidate rules of CAR costimulatory signaling and to guide the design of non-natural costimulatory domains with improved phenotypes, both in vitro and in vivo. Costimulatory signaling modulates the outcome of CAR T cell activation, making costimulatory domains attractive engineering targets for customizing or improving cell therapies. Thus far, costimulatory domain engineering has mostly been limited to the addition of intact natural domains such as those from 4-1BB, CD28, or the interleukin-2 receptor beta subunit (IL2Rβ), effectively using naturally occurring signaling sentences (motif

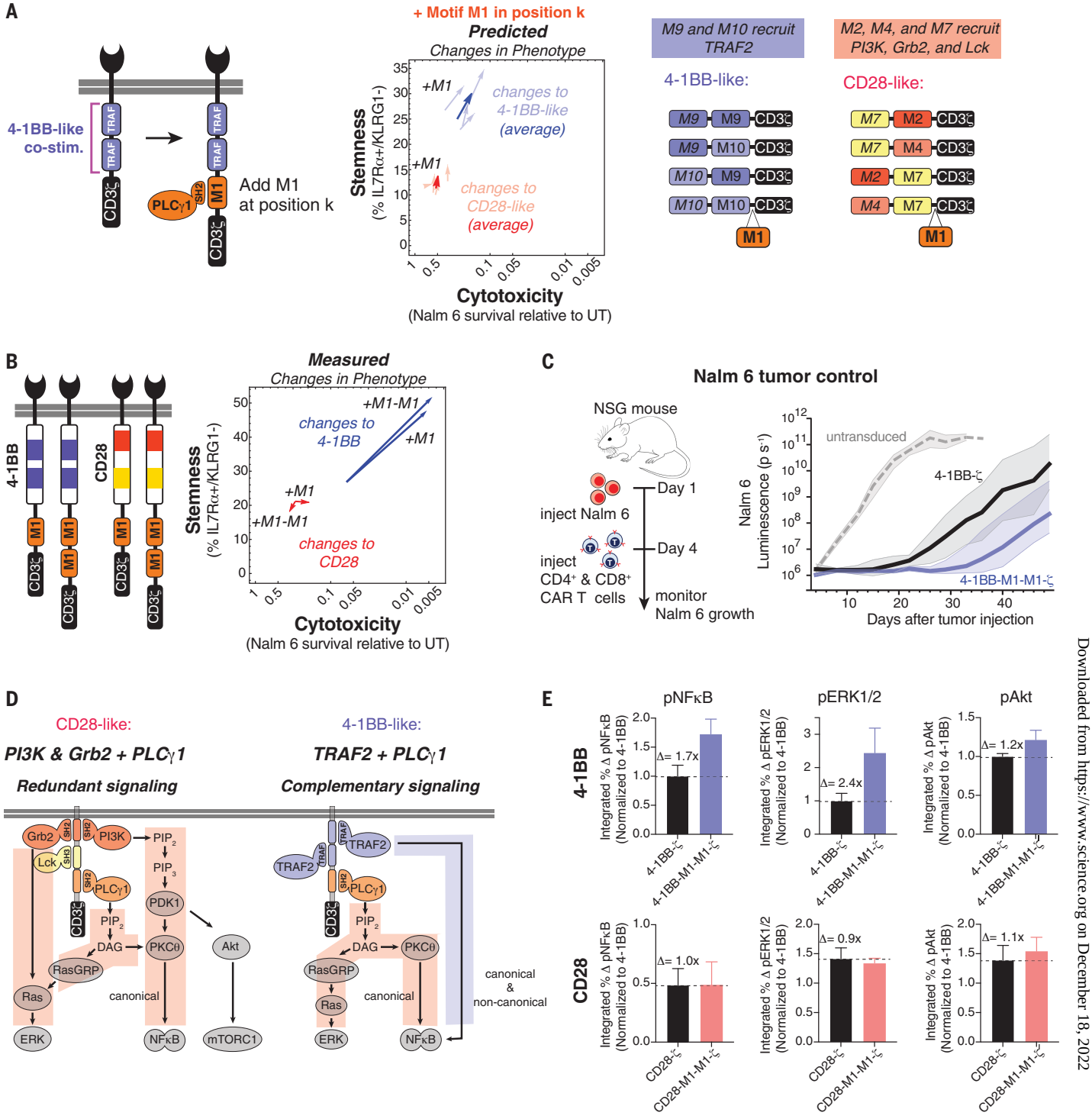

Fig. 4. Neural networks accurately predict that PLCγ1 binding motifs improve the cytotoxicity and stemness of 4-1BB–ζ but not CD28–ζ. (**A**) Library parts that share consensus signaling motifs with 4-1BB and CD28 costimulatory domains were used to predict the effect of adding M1 to 4-1BB and CD28. (**B**) Addition of one or two copies of M1 improved in vitro cytotoxicity and stemness of 4-1BB–ζ but not CD28–ζ. CAR T cell cytotoxicity and stemness were assessed after four pulses of Nalm 6 cells. Data are means of n = 3 to 5 replicates. (**C**) $CD4^+$ and $CD8^+$ CAR T cells were sorted for CAR expression 6 days after activation (1 day after Dynabead removal) and injected into mice 10 days later. NSG mice were injected intravenously with 0.5×10^6 Nalm 6 cells and then injected intravenously with 3×10^6 CAR^+ T cells on day 4. CAR T cells with 4-1BB–M1–M1–ζ showed improved early tumor control relative to 4-1BB–ζ. Traces in (C) are median luminescence ± SEM confidence interval. (**D**) Costimulatory PLCγ1 signaling is redundant to signaling provided by PI3K and Grb2 but complementary to TRAF signaling. (E) Addition of M1 to 4-1BB–ζ induced modest changes in Akt phosphorylation, which is not downstream of PLCγ1 signaling, relative to the changes in ERK1, ERK2 and NFκB phosphorylation, which are downstream of PLCγ1 signaling. $CD4^+$ and $CD8^+$ CAR T cells were pulsed once with Nalm 6 leukemia cells and fixed at various time points from 0 to 60 min. Phosphorylation of ERK1 and ERK2, NFκB, and Akt was assessed by flow cytometry. Data for (**E**) are means and standard deviation of n = 3 replicates. p, phosphorylated.

combinations). We used motifs from receptors as words to generate thousands of different signaling sentences that drove T cells to distinct cell fates, potentially yielding more diverse and nuanced phenotypic meaning. Augmenting experimental analysis of a subset of receptors with neural network analysis allowed us to explore a larger region of combinatorial motif space. In particular, we identified the non-natural combination of TRAF- and PLCγ1-binding motifs that may be useful in CAR T cell therapies. With an arrayed screen of several hundred receptors and machine learning, we identified basic elements of signaling motif language and extracted design rules that relate motif combinations to cell fate. This represents a step toward forward engineering receptors with desired properties. Similar screening approaches with other CARs and target cancer cells are needed to determine the optimal signaling domains for each CAR and tumor type. Libraries may also be of use in identifying combinations of binding, hinge, linker, transmembrane, and signaling domains that produce optimal T cell function and assessing the safety and toxicity of such combinations. Exploration of these larger libraries may benefit from machine learning owing to the size and complexity of the combinatorial space. Machine learning–augmented screens of this type might be used to engineer many other classes of receptors for biological research and cell therapy applications that involve cellular processes controlled by combinations of signaling motifs.

REFERENCES AND NOTES

1. D. M. Barrett, N. Singh, D. L. Porter, S. A. Grupp, C. H. June, *Annu. Rev. Med.* **65**, 333–347 (2014).
2. B. A. Irving, A. Weiss, *Cell* **64**, 891–901 (1991).
3. C. Romeo, B. Seed, *Cell* **64**, 1037–1046 (1991).
4. F. Letourneur, R. D. Klausner, *Proc. Natl. Acad. Sci. U.S.A.* **88**, 8905–8909 (1991).
5. A. Krause *et al.*, *J. Exp. Med.* **188**, 619–626 (1998).
6. H. M. Finney, A. D. G. Lawson, C. R. Bebbington, A. N. C. Weir, *J. Immunol.* **161**, 2791–2797 (1998).
7. C. Imai *et al.*, *Leukemia* **18**, 676–684 (2004).
8. C. A. Ramos *et al.*, *Mol. Ther.* **26**, 2727–2737 (2018).
9. G. Enblad *et al.*, *Clin. Cancer Res.* **24**, 6185–6194 (2018).
10. Y. Kagoya *et al.*, *Nat. Med.* **24**, 352–359 (2018).
11. C. A. Koch, D. Anderson, M. F. Moran, C. Ellis, T. Pawson, *Science* **252**, 668–674 (1991).
12. M. Sudol, *Oncogene* **17**, 1469–1474 (1998).
13. O. U. Kawalekar *et al.*, *Immunity* **44**, 380–390 (2016).
14. K. S. Gordon *et al.*, *Nat. Biomed. Eng.* **6**, 855–866 (2022).
15. D. B. Goodman *et al.*, *Sci. Transl. Med.* **14**, eabm1463 (2022).
16. R. Castellanos-Rueda *et al.*, *Nat. Commun.* **13**, 6555 (2022).
17. H. Dinkel *et al.*, *Nucleic Acids Res.* **40**, D242–D251 (2012).
18. J. C. D. Houtman *et al.*, *Biochemistry* **43**, 4170–4178 (2004).
19. Mj. Xu, R. Zhao, Z. J. Zhao, *J. Biol. Chem.* **275**, 17440–17446 (2000).
20. M. Borsa *et al.*, *Sci. Immunol.* **4**, eaav1730 (2019).
21. D. Herndler-Brandstetter *et al.*, *Immunity* **48**, 716–729.e8 (2018).
22. H. Wu *et al.*, *J. Immunother. Cancer* **9**, e002662 (2021).
23. E. B. M. Remmerswaal *et al.*, *Eur. J. Immunol.* **49**, 694–708 (2019).
24. S. P. Schoenberger, R. E. M. Toes, E. I. H. van der Voort, R. Offringa, C. J. M. Melief, *Nature* **393**, 480–483 (1998).
25. S. M. McWhirter *et al.*, *Proc. Natl. Acad. Sci. U.S.A.* **96**, 8408–8413 (1999).
26. H. H. Park, *Front. Immunol.* **9**, 1999 (2018).
27. K. M. Knudson *et al.*, *Proc. Natl. Acad. Sci. U.S.A.* **114**, E1659–E1667 (2017).
28. A. Basant, M. Way, *eLife* **11**, e74655 (2022).
29. L. Zeng, I. Palaia, A. Šarić, X. Su, *J. Cell Biol.* **220**, e202009154 (2021).

ACKNOWLEDGMENTS

We thank S. Levinson for sharing tumor cell lines, I. Webster of Zenysis Technologies for assistance with processing sequencing data, R. Almeida and other members of the Lim lab for helpful discussions, and W. Maestas and J. Fraser for critical reading of this manuscript. **Funding:** This work was supported by a Burroughs Wellcome Fund Postdoc Enrichment Program Fellowship to K.G.D.; a Damon Runyon Cancer Research Foundation Fellowship to K.G.D.; an IBM Exploratory Life Science program grant to S.W., S.C., and S.B.; and NSF Center for Cellular Construction grant DBI-1548297. Research reported in this publication was supported by the National Cancer Institute of the National Institutes of Health under award number U54CA244438 and R01 CA249018 to W.A.L. The content is solely the responsibility of the authors and does not necessarily represent the official views of the National Institutes of Health. **Author contributions:** K.G.D. and W.A.L. designed research. S.W., K.G.D., and S.B. designed the artificial intelligence (AI) research. K.G.D., H.K.B., M.S.S., Y.T., W.Y., and S.W. performed research. K.G.D., S.W., and W.A.L. contributed new reagents or analytic tools. K.G.D. and S.W. analyzed data. S.B., S.C., and W.A.L. contributed research guidance and supervision. K.G.D. and W.A.L. wrote the paper. All authors edited the paper. **Competing interests:** A provisional patent application has been filed by the University of California related to this work (US application number 63/279,578). W.A.L. is on the scientific advisory board for Allogene Therapeutics and is a shareholder of Gilead Sciences and Intellia Therapeutics. **Data and materials availability:** Reagents are available from the corresponding author upon request from the authors. The pHR plasmid containing the anti-CD19 CAR and plasmids containing DNA for the 13 motifs used in the combinatorial library will be available from Addgene. Array screening data are available in supplemental information. Machine-learning data analysis codes are available at https://github.com/CCCofficial/combinatorial_signaling_motif_libraries.

SUPPLEMENTARY MATERIALS

science.org/doi/10.1126/science.abq0225
Materials and Methods
Figs. S1 to S7
Tables S1 and S2
References (*30*–*32*)
MDAR Reproducibility Checklist
Data S1 to S3

View/request a protocol for this paper from *Bio-protocol*.

Submitted 13 March 2022; accepted 18 November 2022
Published online 8 December 2022
10.1126/science.abq0225

Decoding CAR T cell phenotype using combinatorial signaling motif libraries and machine learning

Kyle G. DanielsShangying WangMilos S. SimicHersh K. BhargavaSara CapponiYurie TonaiWei YuSimone BiancoWendell A. Lim

Science, 378 (6625), • DOI: 10.1126/science.abq0225

Exploring receptor design principles

Chimeric antigen receptor T cell technology, in which cells of the immune system are modified with customized receptors, has proved effective in cancer therapy. To explore the range of cell responses that can be encoded in such receptors and to make their design more quantitative and predictive, Daniels *et al*. tested about 200 of 2400 possible combinations of 13 signaling motifs found in such receptors and used machine learning to predict other effective combinations. Using these design rules, the authors constructed receptors in human T cells with improved signaling characteristics that contributed to better tumor control in a mouse model. —LBR